JOURNAL OF GEOPHYSICAL RESEARCH, VOL. 99, NO. D11, PAGES 22,897–22,914, NOVEMBER 20, 1994

Modeling of mineral dust in the atmosphere: Sources, transport, and optical thickness

Ina Tegen
Department of Applied Physics, Columbia University, New York

Inez Fung[1]
NASA Goddard Institute for Space Studies, New York

Abstract. A global three-dimensional model of the atmospheric mineral dust cycle is developed for the study of its impact on the radiative balance of the atmosphere. The model includes four size classes of mineral dust, whose source distributions are based on the distributions of vegetation, soil texture and soil moisture. Uplift and deposition are parameterized using analyzed winds and rainfall statistics that resolve high-frequency events. Dust transport in the atmosphere is simulated with the tracer transport model of the Goddard Institute for Space Studies. The simulated seasonal variations of dust concentrations show general reasonable agreement with the observed distributions, as do the size distributions at several observing sites. The discrepancies between the simulated and the observed dust concentrations point to regions of significant land surface modification. Monthly distribution of aerosol optical depths are calculated from the distribution of dust particle sizes. The maximum optical depth due to dust is 0.4-0.5 in the seasonal mean. The main uncertainties, about a factor of 3-5, in calculating optical thicknesses arise from the crude resolution of soil particle sizes, from insufficient constraint by the total dust loading in the atmosphere, and from our ignorance about adhesion, agglomeration, uplift, and size distributions of fine dust particles ($< 1\,\mu$m).

1. Introduction

One of the largest uncertainties in the modeling of global climate change is the radiative forcing of aerosols. Investigations of the forcing of sulfate aerosols [*Charlson et al.*, 1991; *Kiehl and Briegleb*, 1993] conclude that the radiative effect of sulfate aerosol is about -0.5 $W\,m^{-2}$, which is comparable to a forcing of about +2 $W\,m^{-2}$ by greenhouse gases. No systematic investigations have yet been made of the possible influence of atmospheric mineral dust on the radiation budget, although it has been recognized that in some regions, dust can contribute the major part of aerosol mass loading. Typically, mineral dust is injected into the atmosphere by surface winds from dry soils where the vegetative cover is low and sparse. The lifetime of dust in the atmosphere is dependent on particle size; it may vary between 1 hour for large particles and several years for stratospheric particles. Estimates of the global source of mineral aerosol range between 200 and 5000 $Mt\,yr^{-1}$ [*Goudie*, 1983]. Dust loading in the atmosphere is highly variable in space and time, so that its actual distribution and global impact is difficult to quantify.

The radiative effect of mineral aerosols would probably be underestimated if the global/annual mean dust concentrations in the atmosphere were assumed to be given by those measured at coastal or remote observing sites. Instead, regional and seasonal variations in the dust distribution are likely to be important in calculations of the radiation budget. Since the radiative effects of aerosols depend on their particle sizes, both the total mass loading and the size distribution of dust particles have to be determined. Existing models of the cycle of atmospheric dust [*Genthon*, 1992; *Joussaume*, 1990] do not provide realistic seasonal variations and do not include particle size distributions.

In this paper we present a new model of the distribution of atmospheric mineral dust that takes into account the size distribution of the dust particles. The dust source and sink parameterizations were mainly based on empirical data sets and the dust transport is simulated in a three-dimensional atmospheric tracer model derived from a general circulation model. The resulting optical thickness distributions are derived from the resultant size distributions. The sensitivity of optical thickness to model assumptions about dust sources are presented.

[1] Also at School of Earth and Ocean Sciences, University of Victoria, British Columbia, Canada.

Paper number 94JD01928.
0148-0227/94/94JD-01928$05.00

2. Modeling

The mineral dust model is shown schematically in Figure 1. At the source the size distribution of soil particles is characterized by four particle size classes representing clay, small silt, large silt, and sand. For each size fraction the soil mass is uplifted by surface wind and transported by the large-scale atmospheric circulation. The deposition processes are gravitational sedimentation, turbulent mixing, and wet deposition by rain, with the removal efficiencies dependent on the particle size. For sand particles, gravitational settling alone determines the sedimentation velocity, while for clay particles, gravitational sedimentation is negligible compared to the other removal processes. The components of the model are described in detail below.

2.1. Particle Sizes

The size distribution of mineral dust is crucial for the determination of aerosol radiative impacts. Existing data sets of soil properties report soil texture as mixtures of "clay" (particle diameter less than 2 μm), "silt" (particle diameter between 2 and 50 μm), and "sand" (particle diameter between 50 and 2000 μm). No finer resolution of particle sizes is available at this time on a global scale. The soil data sets give the mass fraction for the individual soil classes but do not provide information about the mass distribution between the upper and the lower size limit.

We used the $1^\circ \times 1^\circ$ data set of soil types and particle sizes [*Zobler*, 1986; *Webb et al.*, 1991], where the fractions of the three major size classes are given as percentages of total soil mass in each grid box. While the sizes in the soil data set are given as diameters, measurements of atmospheric aerosols are reported in terms of particle radii. We therefore use in the following the radius instead of the diameter to characterize the particle sizes.

Because of the dependence of particle lifetimes in the atmosphere on their sizes (the removal of particles larger than 10 μm (radius) is mainly determined by their gravitational settling velocity) we divided the silt fraction into a "small silt" fraction between 1 and 10 μm and a "large silt" fraction between 10 and 25 μm radius. The lifetime of small silt in the atmosphere lies in the order of days while the lifetime of large silt lies in the order of hours, therefore only one "silt" particle class would not be justified for dust transport calculations.

To calculate the source strength of the mineral aerosol, the portion of the mass fraction that is available for dust uplift must be determined for each size class. The assumptions that we made about particle size distributions and the erodible fractions of the soil are shown schematically in Figure 2 and described below.

2.1.1. Clay. The smallest clay particle radius measured is about 0.01 μm [*Scheffer and Schachtschabel*, 1992]. The particle sizes appear to follow a lognormal size distribution [*U.S. Depaprtment of Agriculture (USDA)*, 1975]. The number distribution of clay particles can be described by $dN/d\log r \propto r^{-3}$ or $dN/dr \propto r^{-4}$, the corresponding mass distribution follows $dM/d\log r = \text{const}$; i.e., the clay mass is distributed approximately equally over logarithmic size intervals. This distribution is corroborated by the similar lognormal size distribution ($dN/d\log r \propto r^{-3}$) [*Junge et al.*, 1969] for aerosols (Junge spectra).

In a wind tunnel experiment, *Gillette et al.* [1974] found that no size fractionation occurred between soil and dust particles for particles with radii larger than 0.5 μm. Similar results were obtained by *d'Almeida and Schütz* [1983] in air filter and soil size measurements: they found that size distributions in dust and corresponding soil samples were similar down to a size of about 0.3–0.7 μm.

With decreasing particle size, the adhesive and cohesive forces of the particles increase due to their increased surface area. As a result clay particles tend to agglomerate and to stick to larger particles [*Scheffer and Schachtschabel*, 1992], thus leading to a decreased availability of small clay particles for wind erosion. The

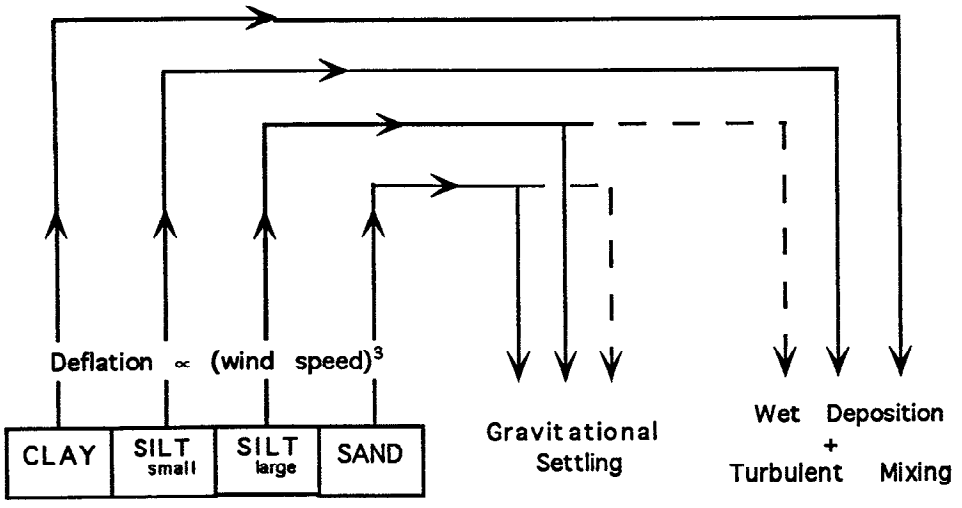

Figure 1. Schematic description of the dust transport model.

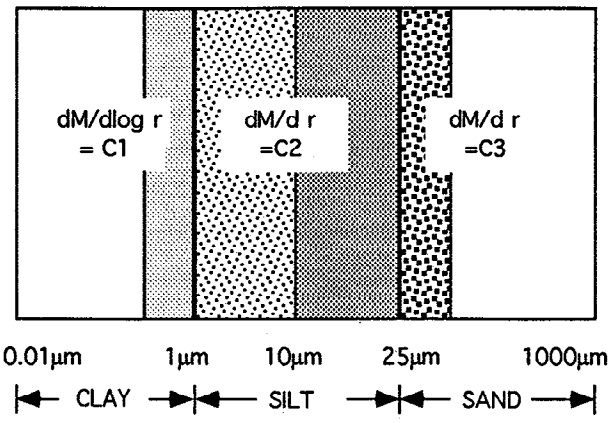

Figure 2. Assumed mass distributions for dust model as a function of soil particle radius; shaded regions indicate the size range of the four soil particle classes available for dust uplift.

mass of dust particles with smaller sizes decreases by 2 orders of magnitude relative to the mass of soil particles in the same size range. This means that we must assume a minimum particle size for clay particles that can be uplifted by surface wind.

Measurements of size spectra of mineral aerosol as reported by [e.g., *Prospero and Bonatti,* 1969; *d'Almeida and Schütz,* 1983] show the mass of clay particles to be 1–2 orders of magnitude smaller than the mass of silt particles (1–10 μm). That would mean that a fraction of the clay particles smaller than some critical radius is not available for wind erosion as individual particles, probably due to agglomeration and adhesive bindings of clay particles in the soil. However, no information is available about the magnitude of this effect.

To take these uncertainties into account we chose the following cases as extreme assumptions for the clay source strength in the dust model:

1. All of the clay particles with radii larger than 0.4 μm are available for wind erosion as individual particles; no particle with a smaller radius can be mobilized. With a lognormal size distribution this clay fraction represents 1/6 of the total clay mass.

2. Only part of the clay particles with radii larger than 0.4 μm are available for wind erosion. The fraction of erodible clay is chosen in a way that the total clay aerosol mass in our model after 1 modeled year is 1/10 of the total small silt aerosol mass as suggested by measurements of aerosol size spectra [*Prospero and Bonatti,* 1969; *d'Almeida and Schütz,* 1983]. It turns out that this condition implies that 1/50 of the total mass of the clay source must be available for wind erosion.

2.1.2. Silt. The silt mass of the soils was divided in equal parts into small ($1 < r < 10\,\mu$m) and large silt fractions ($10 < r < 25\,\mu$m) (Figure 2). This assumption is justified for most soils [*USDA,* 1975]. For both fractions we assumed $dM/dr = \text{const}$, although a lognormal size distribution ($dM/d\log r = \text{const}$) would also be justified.

2.1.3. Sand. No general size distribution would be justified for sand because of its spatial variability. Sand (as well as large silt) settles rapidly out of the atmosphere, and so its size distribution reflects removal processes rather than the distributions of the source. Only small sand particles are available as atmospheric dust, since large sand particles rapidly fall back to the ground. This means that the size distribution is not important for the sand fraction. From rough estimations of their lifetime in the atmosphere [*Jaenicke,* 1978] we assume the upper limit of the radius of sand particles available as atmospheric dust to be 50 μm. Larger particles have lifetimes in the atmosphere of generally less than 1 hour and have therefore not been considered in the model, although it should be noted that particles with radii of several hundred micrometers have been observed over the North Pacific in a distance of 8000 km from the source region in China [*Betzer et al.,* 1988]. Also "giant" sand particles from North Africa have been found in the Amazon basin [*Swap et al.,* 1992]. These are, however, exceptional cases and those particles are unlikely to influence the mass balance of wind-borne sand. The included fraction of sand (25–50 μm) contains usually between 2 and 25 % of the total sand mass in the soil [*USDA,* 1975].

2.1.4. Particle Properties Table 1 summarizes the range of possible radii and size ranges of the four soil particle classes available for uplift. The wide ranges reflect insufficient knowledge a priori of the size distributions within each soil size class and our limited understanding of the processes involved in the uplift of clay. These uncertainties lead to uncertainties in the modeled dust distributions.

2.2. Dust Sources and Uplift

The crucial factors for the determination of the source strength of mineral aerosols are surface wind speed, soil

Table 1. Model Assumptions for the Different Dust Particle Size Classes

Type	Size Distribution	Size Range, μm	α	Density, g cm^{-3}
Clay	$dM/d\log r = \text{const}$	0.5–1	1/50–1/6	2.5
Silt, small	$dM/dr = \text{const}$	1–10	1	2.65
Silt, large	$dM/dr = \text{const}$	10–25	1	2.65
Sand	$dM/dr = \text{const}$	25–50	1/50–1/4	2.65

α, ratio of the mass available for uplift and the total mass of the respective size class.

water content, and vegetation cover. Disturbance of the soil surface by land use would also alter the source strength but was neglected for this model study.

Wind erosion occurs only on dry soils. In our model we assumed that dust is uplifted if the soil matric potential is higher than $10^4\,\mathrm{J\,kg^{-1}}$, when the soil starts to be hygroscopic [*Scheffer and Schachtschabel,* 1992]. The soil matric potential is dependent on soil moisture and texture and is calculated using the model employed by *Bouwman et al.* [1993]. There, water content at field capacity (SSC) and monthly mean water content (SWC) in the upper 30 cm are determined from monthly climatological rain data [*Shea,* 1986], soil types, and soil texture [*Zobler,* 1986]. *Scheffer and Schachtschabel* [1992] give typical curves of the dependency of soil matric potential on soil moisture for sand, silt, and clay. From these curves we determined the saturation ratio SWC/SSC necessary to obtain a matric potential of $10^4\,\mathrm{J\,kg^{-1}}$ to be 20% of the SSC for sand, 25% for silt, and 50% for clay. With these values we determined the areas of dry soil from the saturation ratio for each month.

Uplift of dust can only occur where the vegetation cover is low and sparse. We used the vegetation cover data set of *Matthews* [1983] to exclude regions with tall vegetation (e.g., forests) as possible dust sources and assumed wind erosion to be possible in desert, grassland, and shrub land regions. With this assumption, 33% of the land surface or 9.5% of the global surface are possible dust source regions.

We excluded snow-covered regions as possible dust sources using monthly mean spatial snow coverage maps, which were extracted from the "C2" data of the International Satellite Cloud Climatology Project (ISCCP) [*Rossow et al.,* 1991].

Several empirical studies show that the amount of uplifted dust follows

$$q_a = C(u - u_{tr})u^2 \qquad (1)$$

[*Gillette,* 1978], where q_a is the dust flux from the surface, u is the surface wind speed, and u_{tr} is a threshold velocity. We chose the threshold surface wind velocity at 10-m height to be $6.5\,\mathrm{m\,s^{-1}}$, corresponding to *Kalma et al.* [1988].

Shao et al. [1993] show that for all particle sizes, dust uplift is effected by large saltating particles which mobilize smaller particles when they impact on the ground. As no fractionation due to particle sizes occurs in this process [*Gillette et al.,* 1974; *d'Almeida and Schütz,* 1983], we assumed the dimensional factor C to be constant for all size classes. C is to be determined a posteriori in this model.

As the dust uplift depends strongly on the surface wind speed, it is essential to use wind data with high resolution in space and time to obtain realistic results. We used Europen Center for Medium Range Weather Forecasting (ECMWF) (Tropical Ocean Global Atmosphere (TOGA) Analysis) wind products (10-m surface winds) with a resolution of $1.125° \times 1.125°$ and 6 hourly time steps. One of the uncertainties in using analyzed wind products is that for potential source areas of wind erosion (mainly deserts), only few wind observations exist. In these regions the wind products are extrapolated via ECMWF model physics from proximate observing sites. Uncertainties in the ECMWF product is described by *Trenberth and Olson* [1988].

We assumed the dust, once uplifted from the ground, to be immediately injected into the first dynamic layer in the atmospheric transport model, without explicit treatment of transport through the boundary layer. By doing this, we treated the atmosphere above the source regions as an infinite reservoir.

2.3. Dry and Wet Deposition

Aerosols are removed from the atmosphere by washout by rain (wet deposition), by gravitational settling, and by turbulent mixing out of the first model layer (dry deposition).

The starting point for the parameterization of wet deposition is the climatological monthly precipitation data set of *Shea* [1986]. As the amount of dust that can be washed out per rain event is limited by the supply of dust in the atmosphere, it turns out that the modeled deposited dust mass is up to 50% higher if we calculated dust washout with monthly mean and spatially averaged rain rates instead of taking into account areal coverage and temporal statistics of rain events. Global precipitation climatologies are not available in finer resolution than monthly means. Therefore we developed a scheme to partition the monthly rainfall totals into individual rain events.

Observations in the tropics suggest that rain events occur where clouds with cloud top temperatures less than 235 K are observed [*Adler et al.,* 1993; *Jankowiak and Arkin,* 1991]. We have extracted cloud fractions and cloud top temperatures between 30°S and 30°N for the years 1989 and 1990 from ISCCP "C1" cloud data [*Rossow et al.,* 1991], which have a spatial resolution of $2.5° \times 2.5°$ and a temporal resolution of 3 hours. For each 3-hour period, we identified rain events with the cloud-top temperature criterion and associated the area of the rain event in each pixel with the cloud fraction. We then computed the mean rain rate for each rain event by dividing the monthly total rainfall for the grid box by the total area-weighted rain duration in the month. This mean rain rate is then assigned to each rain event in the month, thus yielding rainfall frequencies like that observed. With this parameterization, rainfall from clouds with lower cloud tops, such as warm rain showers confined in the trade wind boundary layer, are not explicitly included. Nevertheless, the normalization to the observed monthly total rainfall captures the rain from middle and low clouds but assigns it the temporal statistics and vertical distribution of convective rain. Hence wet deposition may be overestimated for high aerosols and underestimated for low aerosols. Whether these effects compensate remains to be evaluated.

For the extratropics we assumed rain events to take place when the 4 hourly surface pressure is decreasing (as extracted from the Goddard Institute for Space

Studies general circulation model (GISS GCM II) [*Hansen et al.*, 1983]). In those regions we assumed a mean regional coverage per rain event to be 50% of the monthly mean total cloud cover (extracted from the ISCCP C2 cloud data) of the corresponding grid box. With these partitioning schemes we subdivided the monthly mean rain data and obtained the amount of rain and the areal coverage for each time step.

Wet deposition rates are also dependent on the vertical distribution of the rain versus the vertical distribution of the dust. In the tropics we assumed only convective rain events to take place. There, the height of the rain clouds was chosen to be ≈ 10 km, corresponding to the cloud-top temperature of 235 K. In Arctic regions, precipitation is only from stratiform clouds from heights of 2 to 3 km [*Berry et al.*, 1945]. Between these extremes we interpolated the rain height H (in kilometers) using $H = 7 + 4\cos(2\theta)$, where θ is the latitude in degrees. This fit yields rain heights of 4–5 km for midlatitudes, consistent with the report of *Mason* [1957].

The efficiency of aerosol removal by rain is usually described by the scavenging ratio Z, which is defined by

$$Z = C_{\text{rain}}/C_{\text{air}} \tag{2}$$

where C_{rain} is the concentration in rain in grams of dust per kilograms of rainwater and C_{air} is the aerosol concentration in air in units of grams of dust per kilograms of air. *Duce et al.* [1991] uses a scavenging ratio for mineral dust of 200 for the North Atlantic Ocean and 1000 elsewhere. *Buat-Menard and Duce* [1986] report scavenging ratios of 500–1000 for clay–sized mineral particles and about 300 for larger mineral particles in the tropical Pacific Ocean. We chose a rather high value of $Z = 750$ for mineral aerosol, which lies within the range of measurements for clay–sized particles. The global mean atmospheric lifetime for clay particles, for which wet deposition is the predominating removal mechanism, is 12 days for $Z = 1000$, 15 days for $Z = 500$, and 27 days for $Z = 200$ in the model. This shows that the removal of atmospheric dust is not very sensitive to the selection of a scavenging ratio between 500 and 1000. For silt and sand particles the atmospheric lifetime is determined by the dry deposition rather than by wet deposition; therefore for these particles the selection of a scavenging ratio is without consequence.

Dry deposition by gravitational settling and turbulent mixing is modeled as in the work *Genthon* [1992]. The gravitational settling velocity v_{stk} for a particle with the radius r is determined using Stokes law with

$$v_{\text{stk}} = \frac{2\rho r^2}{9\nu g} \tag{3}$$

where ρ is the particle density (2.65 g cm^{-3} for quartz (sand, silt), 2.5 g cm^{-3} for clay), g is the gravitational acceleration, and ν is the air viscosity. We calculated the "representative" settling velocity $\hat{v}_{\text{stk}}$ for a dust loading with a continuous particle size spectrum by using

$$\hat{v}_{\text{stk}} = \frac{\int v_{\text{stk}}(r)\frac{4}{3}\pi\rho r^3 dN/dr dr}{\int \frac{4}{3}\pi\rho r^3 dN/dr dr} \tag{4}$$

[*Giorgi*, 1986]. With the assumed size distributions of

$$dN/d\log r \propto r^{-3} \tag{5}$$

for clay and

$$dN/dr \propto r^{-3} \tag{6}$$

for silt and sand we obtained representative gravitational settling velocities of 0.018 cm s^{-1} for clay (corresponding to a mean effective radius of 0.73 μm), 1.2 cm s^{-1} for "small" silt (corresponding to 6.1 μm), 11 cm s^{-1} for "large" silt (corresponding to 18 μm), and 50 cm s^{-1} for the sand fraction with particle radii < 50 μm (corresponding to a radius of 38 μm).

Table 2 shows the resulting global mean atmospheric lifetimes for the different size classes in the model. The lifetimes vary between 1 hour for sand and 13 days for clay. The lifetimes, if only wet deposition is included, are 14 days for all sizes, reflecting the fact that the size does not influence the wet removal efficiency in the model. The lifetimes, if only dry deposition is included, vary between 275 days for clay and 1 hour for sand. These numbers show that for clay, wet deposition is the main removal process. For large silt and sand, dry deposition (gravitational settling) is determining their atmospheric lifetimes.

The turbulent mixing velocity v_d out of the first atmospheric layer is parameterized by

$$v_d = uC_d \tag{7}$$

where C_d is the drag coefficient and u is the surface wind velocity [*Genthon*, 1992]. For all deposition processes the soil was treated as a perfect sink; no remobilization of settled dust was considered.

Table 2. Modeled Atmospheric Lifetimes for the Different Size Classes

Type	r_{eff}, μm	Modeled Lifetime	Wet Deposition Only, Days	Dry Deposition Only
Clay	0.7	13 days	14	275 days
Silt, small	6	40 hours	14	62 hours
Silt, large	18	4 hours	14	4 hours
Sand	38	1 hour	14	1 hour

2.4. Dust Transport

The dust distribution in the atmosphere was calculated using the three-dimensional GISS tracer transport model ($8° \times 10°$) which is described by [e.g., *Prather et al.*, 1987; *Fung et al.*, 1983], with source and sink terms described above. The model transports the tracer by wind fields and subgridscale mixing parameterization extracted from the $4° \times 5°$ version of GISS GCM is used for advection. The linear upstream scheme is described by *Russell and Lerner* [1981].

The four different size classes of dust were treated as four independent tracers in the model. The source strength for each tracer was specified with an uplift factor C arbitrarily set to 1. Because of the short lifetime of the dust the model was integrated for only a year from an initial condition of zero dust loading.

3. Results

Estimates of the global source of mineral aerosol range between 200 and 5000 Mt yr^{-1} [e.g., *Goudie*, 1983; *Pye*, 1987]. In addition, measurements of the deposition rate into the ocean range, depending on the area, from less than 0.001 to more than 10 g m^{-2} yr^{-1} [*Pye*, 1987; *Duce et al.*, 1991]. The observed dust concentration over the ocean is highly variable. *Prospero and Nees* [1976] reports maximum dust concentrations at Barbados of 5–25 μg m^{-3} in the summer months between 1965 and 1975; in winter the concentration drops below 2 μg m^{-3}. In French Guyana, *Prospero et al.* [1981] report maximum dust concentrations of about 20 μg m^{-3} in the years 1978–1979 in spring. In the South Pacific dust concentrations are below 0.1 μg m^{-3} [*Pye*, 1987]. *Gao et al.* [1992] report maximum dust concentrations in spring at Midway of 4 μg m^{-3}. In the Northwest Pacific the dust concentration can reach 60 μg m^{-3} . [*Pye*, 1987].

Because of the short lifetime of atmospheric dust the model was run for only 13 months. The results were taken from the last 12 modeled months. The scaling of the dust concentration was chosen in such a way that the source strength, deposition rates, and dust concentrations are in best possible agreement with the available data. Nevertheless, as the data are highly variable, source strengths between 1500 and 5000 Mt yr^{-1} still give consistent values for concentrations and deposition rates. Our 'best guess' value is a source strength of 3000 Mt yr^{-1}. For this value we obtain for the dimensional factor C that determines the dependency of the dust source strength on the surface wind speed in equation (1) a value of $C = 0.7\,\mu g\,s^2\,m^{-5}$, with a range between 0.4 and 1.2 $\mu g\,s^2\,m^{-5}$.

Measured atmospheric dust concentrations are usually given in units of mass (dust) per volume (air). The GISS tracer model uses normalized pressure coordinates in the vertical direction, so that the appropriate model unit is that of the mixing ratio (kilogram (dust) per kilogram (air)). As surface air pressure varies by only 5%, the modeled dust mixing ratios near the surface can, to first order, be converted into concentrations by multiplying with the surface air density. The conversion at higher altitudes requires information about the local scale height of the atmosphere.

Figures 3a-3d show the modeled distribution of the total dust concentration in the first dynamic layer ($\approx$ 960 mbar) for the four seasons for the "best guess" case. The geographical distribution of mineral dust reflects the principal source regions: the Sahara Desert, the Arabian Peninsula, Central Asia, North China, and Australia. The seasonality of the dust concentration results from the seasonality of the soil water content (determining the source regions), from the seasonality of the surface wind speed (determining the source strength), the seasonality of precipitation (influencing the removal efficiency), as well as the seasonality of atmospheric circulation.

The model realistically reproduces the Saharan dust plume extending far westward between 0° and 30°N in the winter/spring months. However, measurements of dust concentrations in Barbados and French Guyana [*Prospero and Nees*, 1976; *Prospero et al.*, 1981] and observations of haze frequencies at sea [*McDonald*, 1938] show a seasonal latitudinal shift which follows shift of the inner-tropical convergence zone (ITCZ); i.e., the Saharan dust plume is observed about 10° farther south in the winter months compared to the summer month. The model does not reproduce this seasonal shift. A reason for this shortcoming of the model could be the exclusion of human-influenced sources of mineral dust, such as newly exposed soil surfaces due to overgrazing and desertification. This would increase the significance of the Sahel as dust source compared to the Sahara.

The model produces high dust concentrations above the Arabian Sea in summer in good agreement with all observations [e.g., *McDonald*, 1938; *Sirokko and Sarntheim*, 1989]. Additionally, the results show maximum dust over China during spring and maximum over India in June/July, which is also in agreement with observations of dust storm frequencies in these regions [*Littmann*, 1991; *Gao et al.*, 1992].

Figures 4a-4d show the annual mean concentration of the individual dust fractions (clay, small silt, large silt, and sand). The relative amount of smaller particles to larger particles increases with increasing distance from the sources as the larger particles are removed more quickly due to their higher settling velocity. Because of their longer lifetime the distribution of small particles is also more diffuse.

Figures 5a-5d show the modeled vertical distribution in the concentration of the individual tracers as annual mean averaged over all longitudes. The concentrations are given in units of kilogram (dust) per kilogram (air). The vertical structure of dust in our model exhibits an increased concentration of smaller particles relative to larger particles with height, due to the higher sedimentation velocity of the larger particles. The model transports clay and small silt particles into the upper levels of the troposphere by dry and moist convection. The competition between mixing and rainout is clearly seen in the clay distribution outside the ITCZ. As the gravitational settling velocity of clay particles is very small

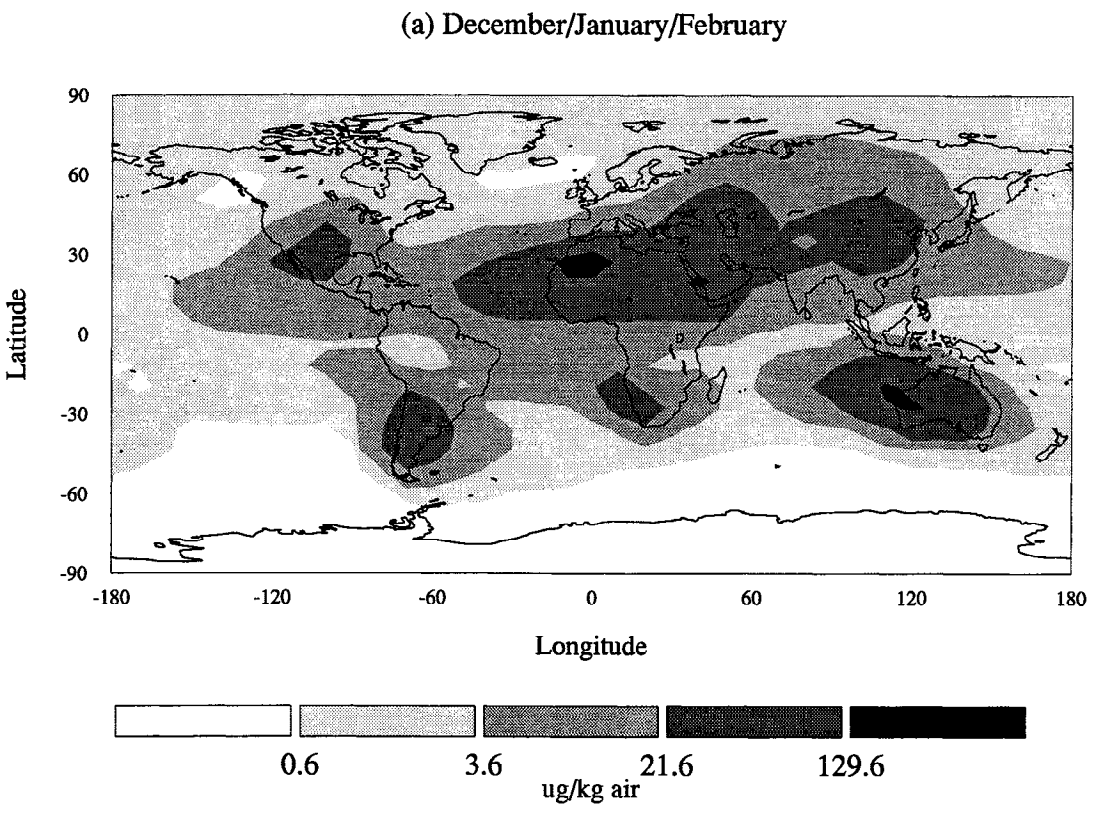

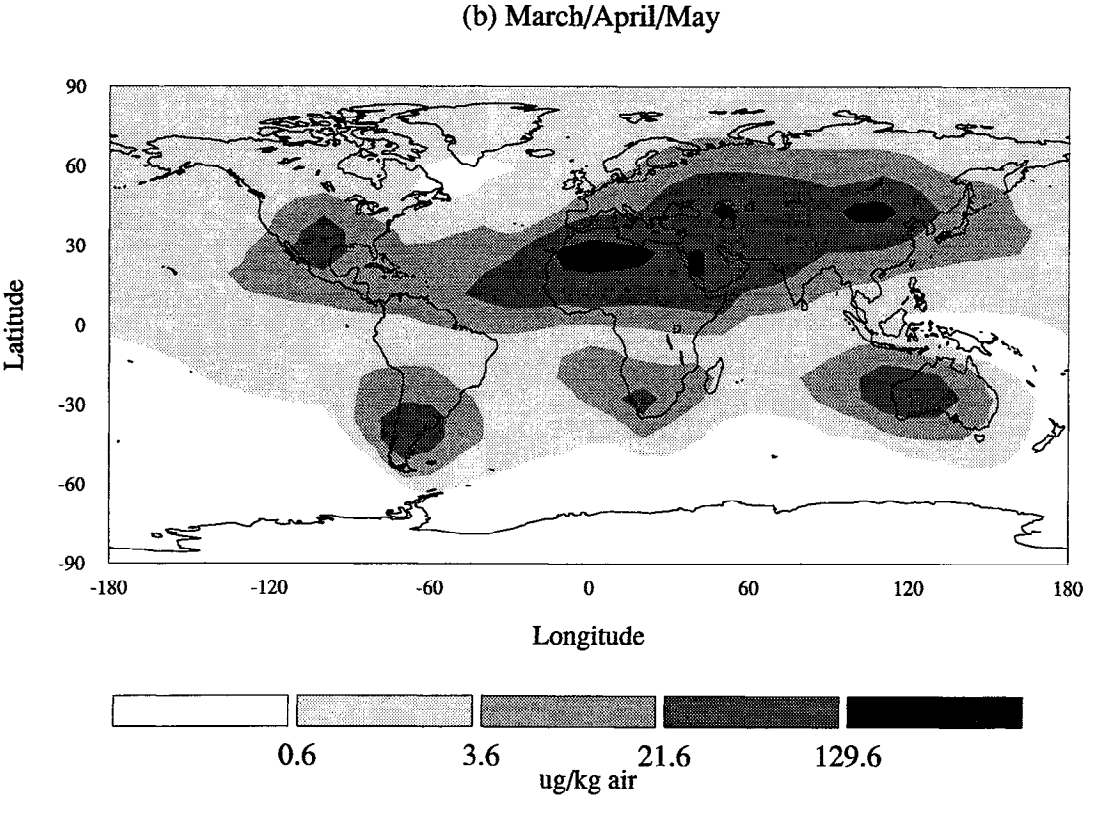

Figure 3. Modeled total dust concentration in the first dynamic model layer for the four seasons. (a) December–February, (b) March–May, (c) June–August, and (d) September–November.

(c) June/July/August

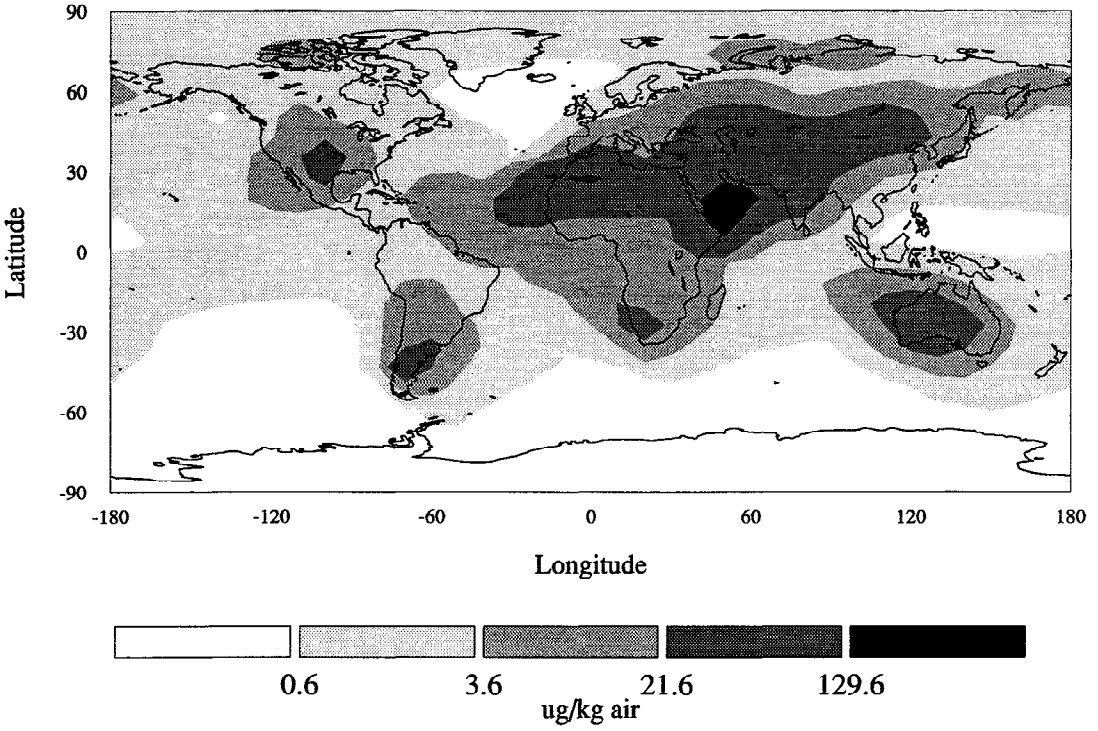

(d) September/October/November

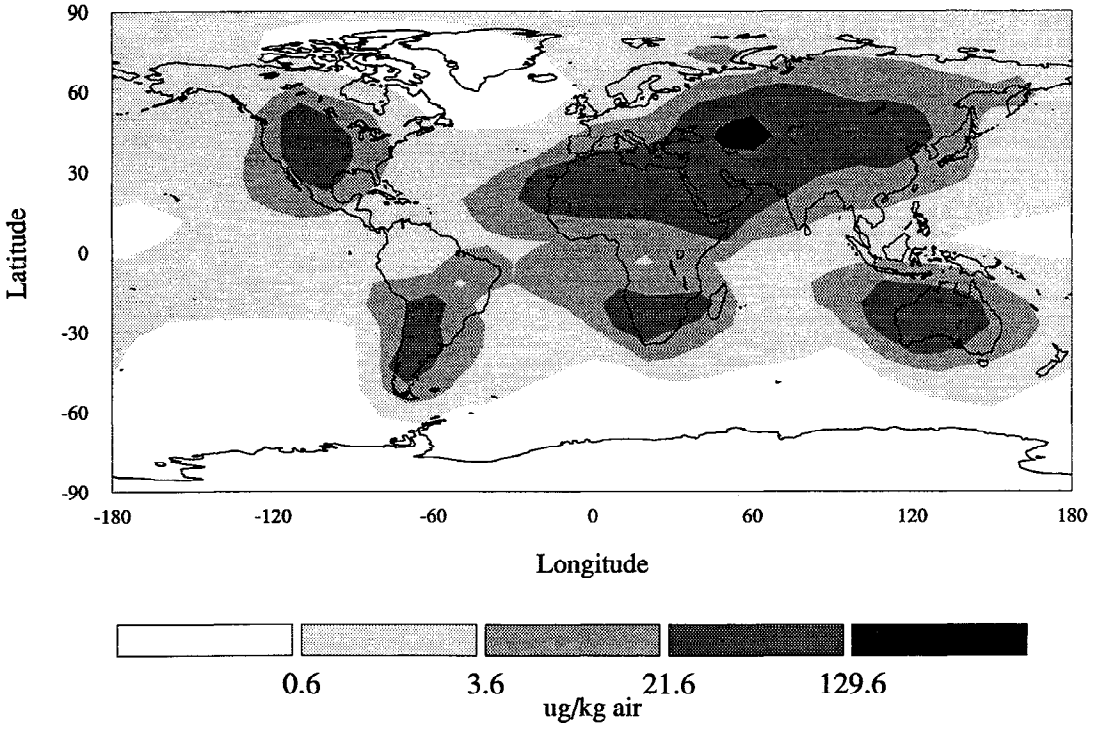

Figure 3. (continued)

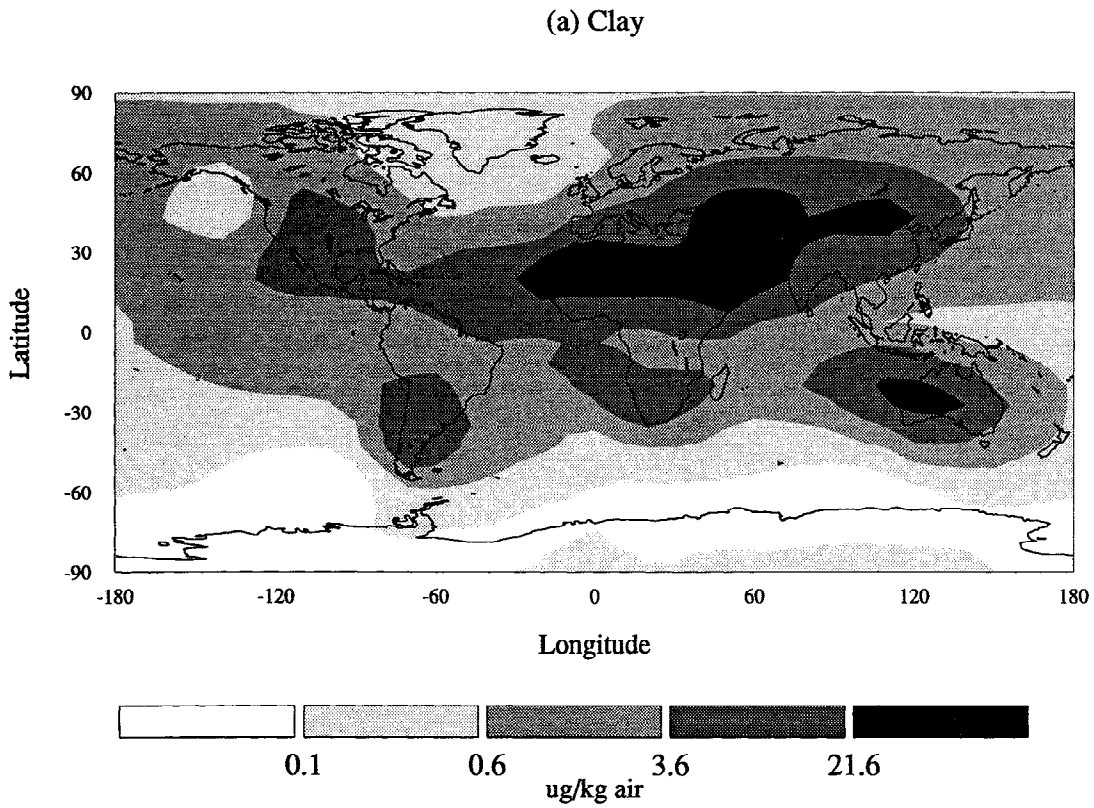

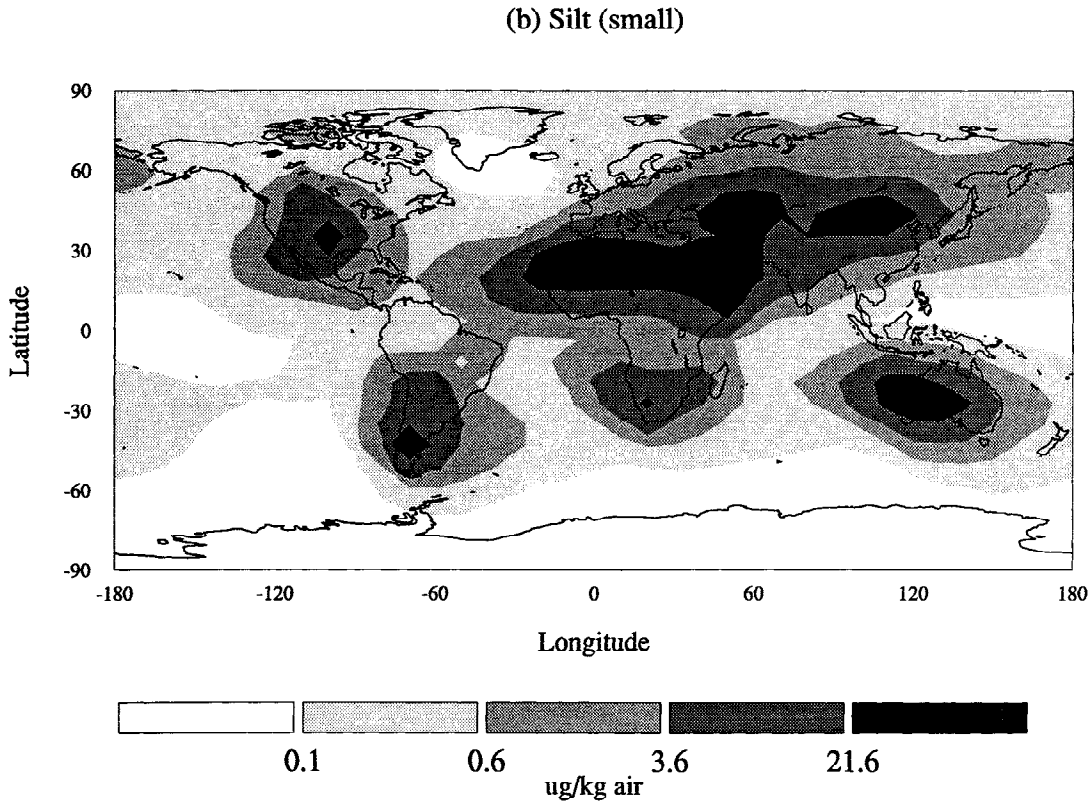

Figure 4. Modeled annual mean dust concentration in the first dynamic model layer for the four different size classes. (a) Clay ($< 1\,\mu$m), (b) small silt (1–10 μm), (c) large silt (10–25 μm), (d) sand ($> 25\,\mu$m).

(c) Silt (large)

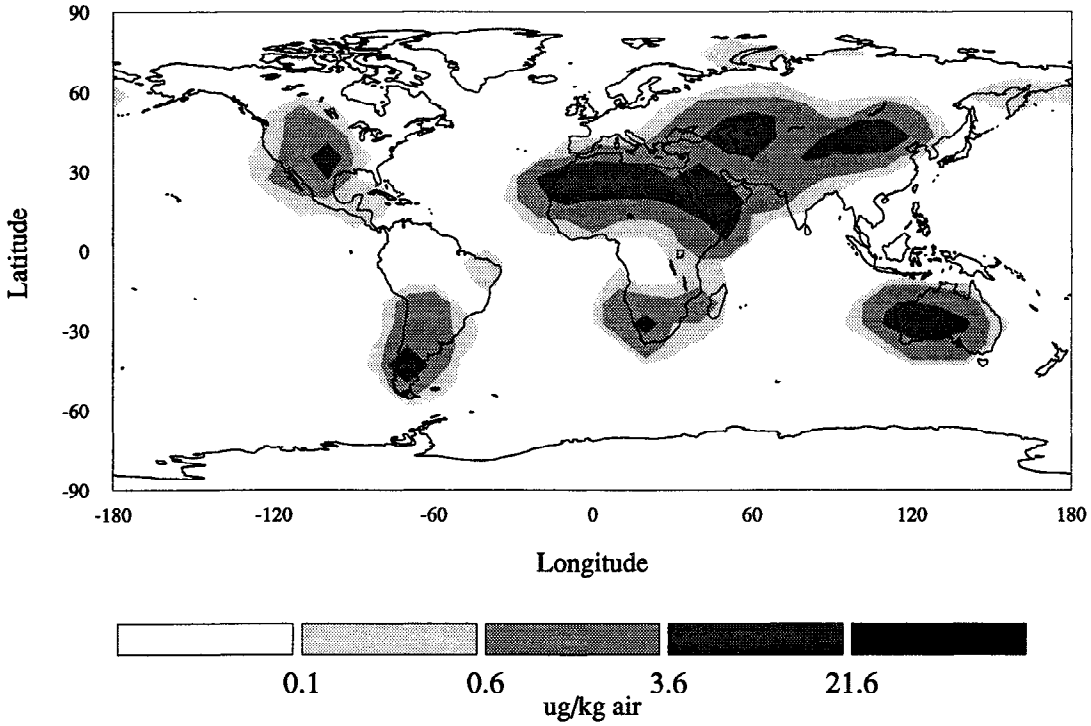

(d) Sand

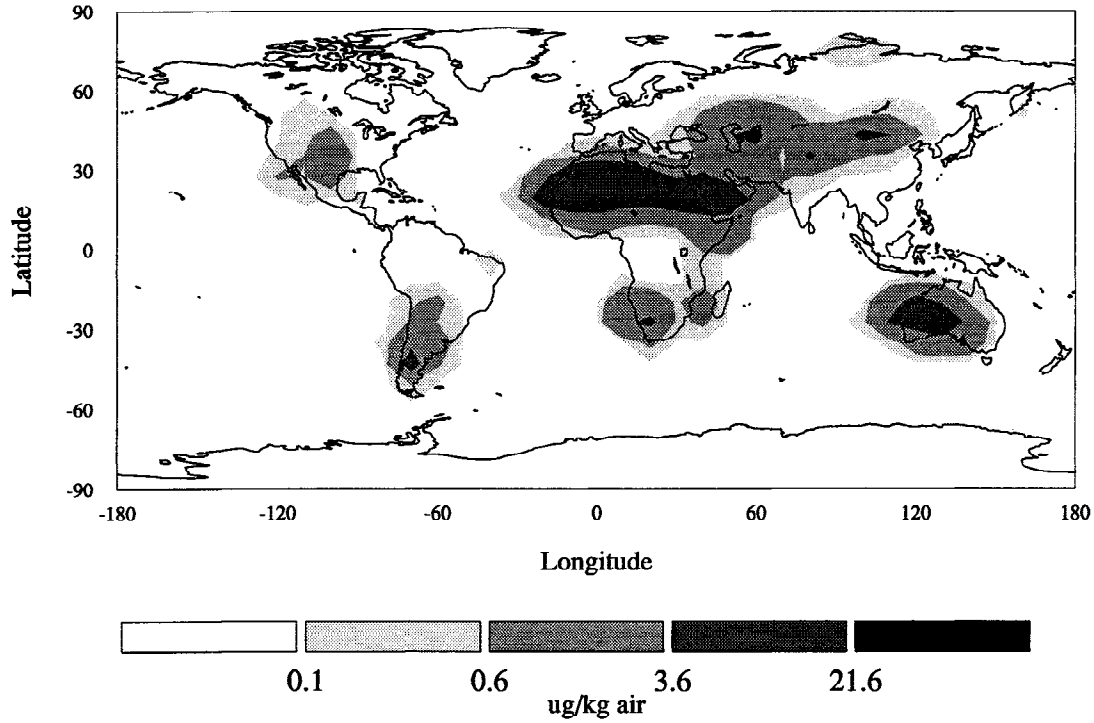

Figure 4. (continued)

($0.018\,\mathrm{cm\,s^{-1}}$) we find a relative increase of clay concentration above the height that is affected by wet deposition outside of the source regions.

Figure 6a shows the total dust mass deposition per year of all size classes in units of grams per square meter and year. The modeled deposition rates range between 0.01 and 120 $\mathrm{g\,m^{-1}\,yr^{-1}}$. These values are in good agreement with mineral dust deposition rates into the oceans given by *Duce et al.* [1991]. The main differences are that the model underestimates the dust deposition into the Pacific east of China (1-10 $\mathrm{g\,m^{-1}\,yr^{-1}}$) and overestimates the deposition west of Australia (10-100 $\mathrm{g\,m^{-1}\,yr^{-1}}$) by a factor of 10, respectively, compared to *Duce et al.* [1991].

Figure 6b shows the ratio of wet deposition flux versus dry deposition flux of dust (without sedimentation) in the model. On the global scale dry deposition is a more important removal process with respect to dust mass than wet deposition because a major part of dust deposition occurs near the source areas, which are arid or semiarid regions with low rain rates. Nevertheless in regions with higher rain rates and weak turbulent mixing (e.g., oceans in midlatitudes), wet and dry deposition are of similar order of magnitude and wet deposition can exceed dry deposition up to a factor of 4.

3.1. Optical Thickness and Particle Sizes

To estimate the influence of the mineral aerosol distribution on the global radiation budget, the optical thickness τ of the dust concentration has to be determined. To first order, the optical thickness is calculated with

$$\tau = Q\pi\hat{r}^2 N \tag{8}$$

$$M = \frac{4}{3}\pi\rho\hat{r}^3 \tag{9}$$

where N is the number of particles, ρ is the particle density, $\hat{r}$ is a representative particle size, and Q is an extinction geometry factor with $Q \approx 2$ for large particles [*Fouquart et al.*, 1987]. As τ is proportional to the number of particles in the air column, the smaller (clay) particles produce a much larger optical thickness per unit mass than the larger (silt) particles. To determine the "effective" particle size for the optical thickness calculation from the continuous size spectra, we used

$$\tau = \frac{3QM}{4\rho\hat{r}} = \int Q\pi r^2 dN/dr\,dr \tag{10}$$

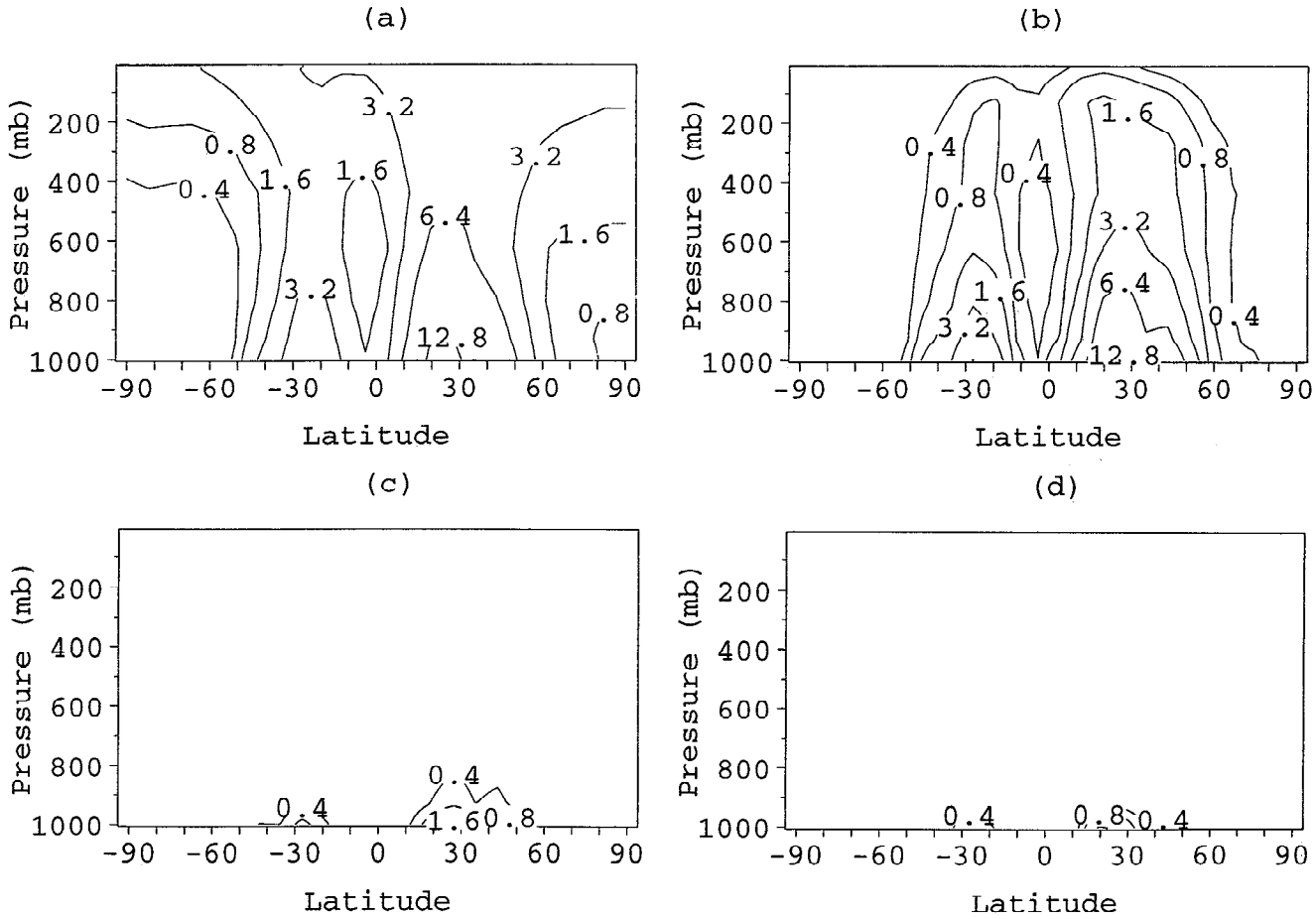

Figure 5. Vertical distribution of dust concentration for the four different size classes (averaged over all longitudes) in units of microgram dust per kilogram air. (a) Clay ($< 1\,\mu$m), (b) small silt (1–10 μm), (c) large silt (10–25 μm), (d) sand ($> 25\,\mu$m).

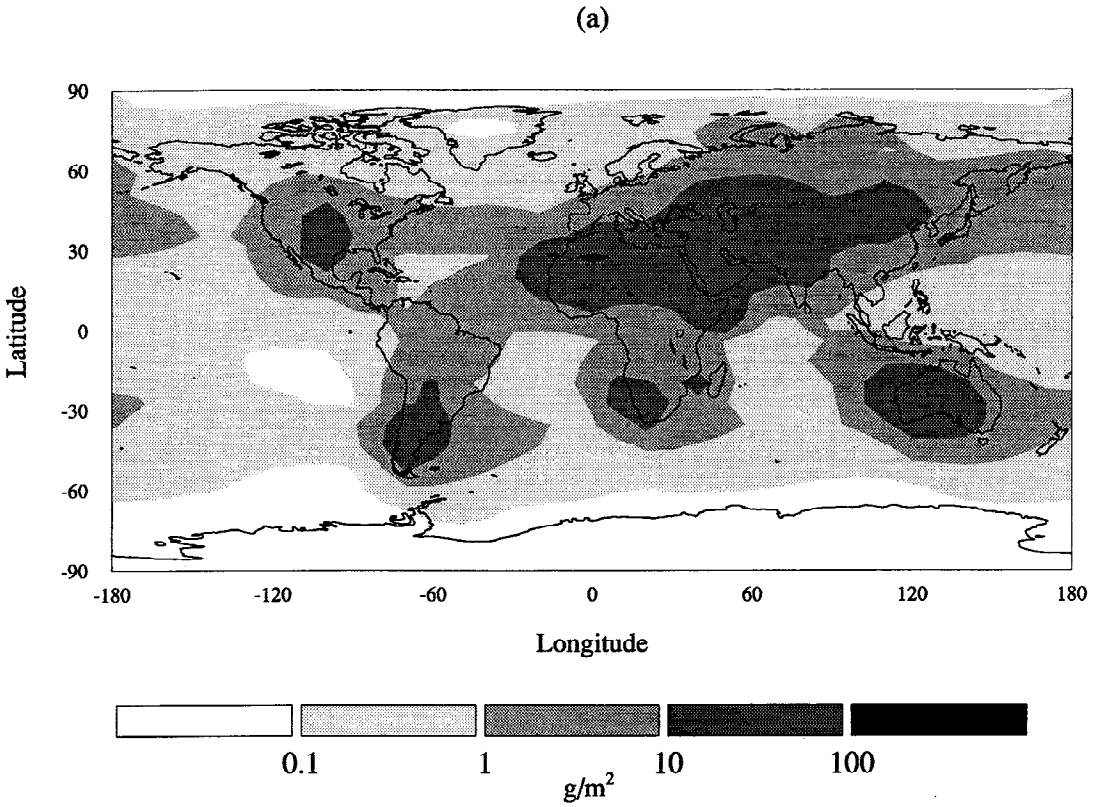

Figure 6. Modeled dust deposition. (a) Total annual dust deposition rates, (b) ratio of wet and dry dust deposition (without sedimentation).

with

$$M = \int \frac{4}{3}\pi\rho r^3 dN/drdr. \quad (11)$$

For clay we obtained with the number size distribution $dN/d\log r \propto r^{-3}$ a representative radius of 0.6 μm if we consider clay particles $\geq 0.4\,\mu$m. For 'small' silt we obtained with the size distribution $dN/dr \propto r^{-3}$ (see above) an effective radius of 4 μm. 'Large' silt and sand have not been taken into consideration for the calculation of the optical thickness since their relative contribution to the total optical thickness is negligible. Figure 7 shows how the uncertainty of the assumption of a minimum clay particle size available as atmospheric dust affects the optical thickness resulting from a certain dust concentration. The range of the representative radii (0.26, 0.5, and 0.7 μm) correspond to assumptions of a minimum radius of 0.1, 0.3, and 0.5 μm, respectively. The resulting optical thickness varies by a factor of 2 due to this assumptions. For silt particles the effective radius for the calculation of optical thickness is tied to the assumption about the size distribution: a distribution

$$dM/dr = \text{const} \quad (12)$$

yields an effective radius of 4 μm, while

$$dM/d\log r = \text{const} \quad (13)$$

yields a representative radius of 2.6 μm. Figure 7 shows that the uncertainty in the optical thickness of dust due to the assumptions about the silt size distribution is negligible compared to the effects of the uncertainties in the processes of clay uplift.

Over the oceans these calculated optical thicknesses can be compared with retrievals of optical depths from the advanced very high resolution radiometer (AVHRR) aboard polar-orbiting weather satellites [*Rao et al.*, 1988]. The AVHRR data show maximal optical depths

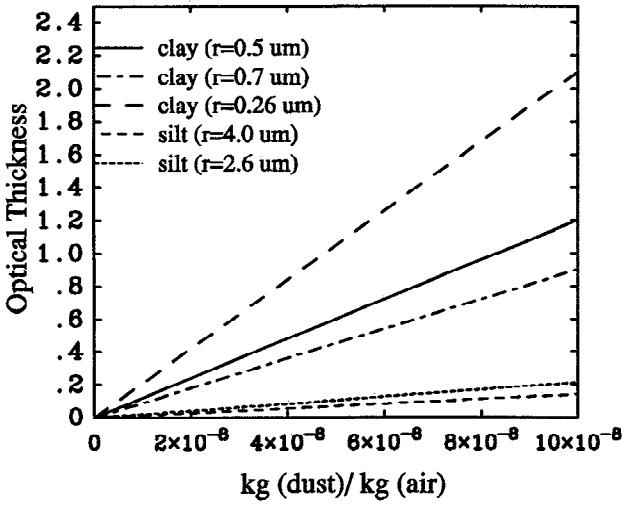

Figure 7. Dependency of optical thickness on the dust concentration considering different "typical" particle sizes.

of about 0.6 to 1.0 in areas with high dust loading (Saharan dust plume, Arabian Sea). Other authors find maxima in optical thickness caused by mineral dust up to 1.5–2 [*Fouquart et al.*, 1987; *Dulac et al.*, 1992; *Jankowiak and Tanre*, 1992]. In remote ocean areas the optical thickness is usually less than 0.1. We note that a strict comparison is not possible because the satellite data are biased toward clear sky conditions and because of assumptions employed in the retrieval algorithm.

Figures 8a-8d show the seasonal distributions of the optical thickness for our "best guess" case. The maximum of the modeled optical thickness is 0.4–0.5 in the seasonal average, which is smaller than retrieved optical thickness maxima. Usually dust events which result in high optical depth take place on the order of days, so that the smaller modeled maximum in optical thickness may be due to the seasonal averaging of our results. On the other hand the lower modeled optical thicknesses may be due to the uncertainties of the assumptions of the processes involved in clay uplift.

As mentioned above, the model does not reproduce the seasonal shift of the Saharan dust plume which is observed in the AVHRR optical thickness data. Also, the model shows Australia as a strong dust source in December to February, which is not seen in the satellite data either. These could be an indication that undisturbed desert areas are relatively weak sources of dust compared to areas influenced by human activity.

Certain assumptions had to be made for the particle size distributions in each size class as well as for the processes involved in the uplift of clay particles, like which fraction of clay is actually carried out of the soil and which is the smallest size of clay particles being uplifted as individual particles. Clay particles are the part of mineral dust which are most important for calculating optical depths.

To show whether our model transports the different size fractions in a realistic way we show in Figures 9a-9d modeled cumulative size frequencies at four different locations compared to dust size measurements at these locations (cited by *Pye* [1987]). At the locations "Arizona", "England, and "Beijing" the size frequencies are reasonably well reproduced by the model, while at the location "Barbados" the model underestimates the small particle fraction (Figure 9d). This implies that the modeled optical thickness may also be underestimated at this location.

To show the influence of the uncertainties of the model assumptions about dust source strength, effective clay radius, and the fraction of the soil that is available for wind erosion on the modeled optical thickness, Table 3 gives the range of the modeled annual average of the optical thickness at four sites which are obtained by varying those factors. Varying the dust source strength between 1500 and 5000 Mt yr^{-1} and varying the effective clay radius between 0.3 and 0.7 μm, leads to an uncertainity of about factor of 3, respectively. A variation of the clay fraction available, as described in Table 1, leads to an uncertainity of the resulting optical thicknesses by about a factor of 5.

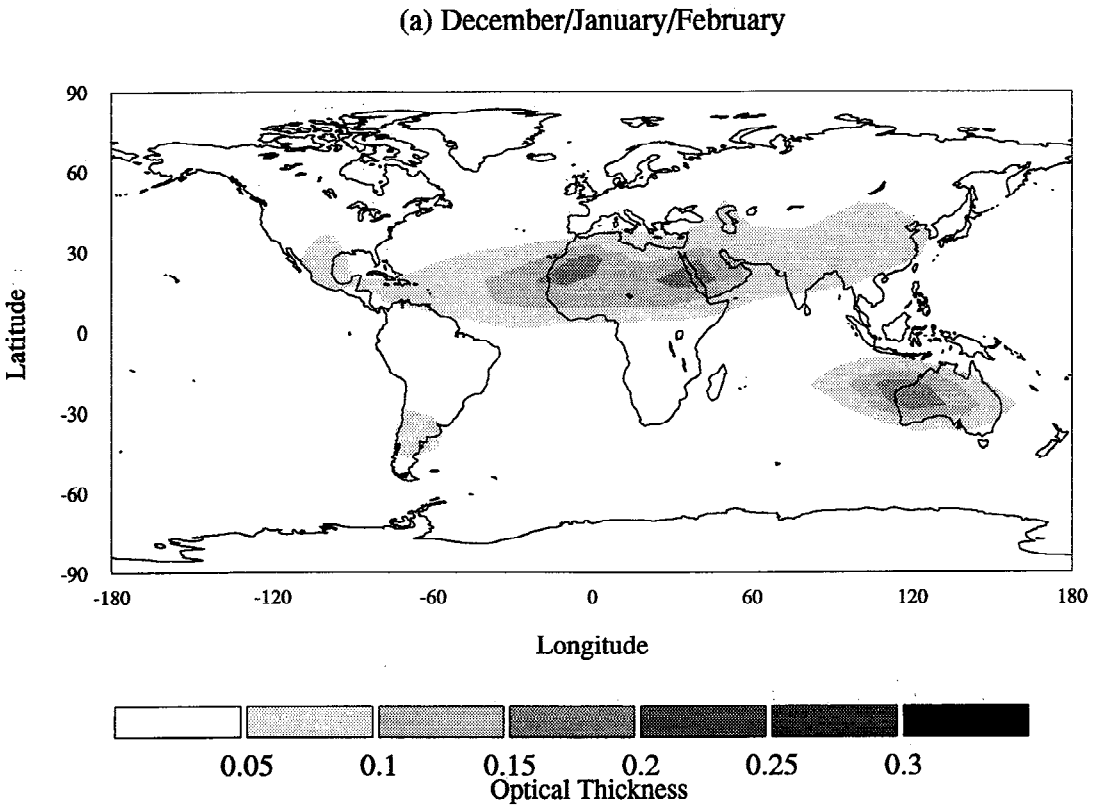

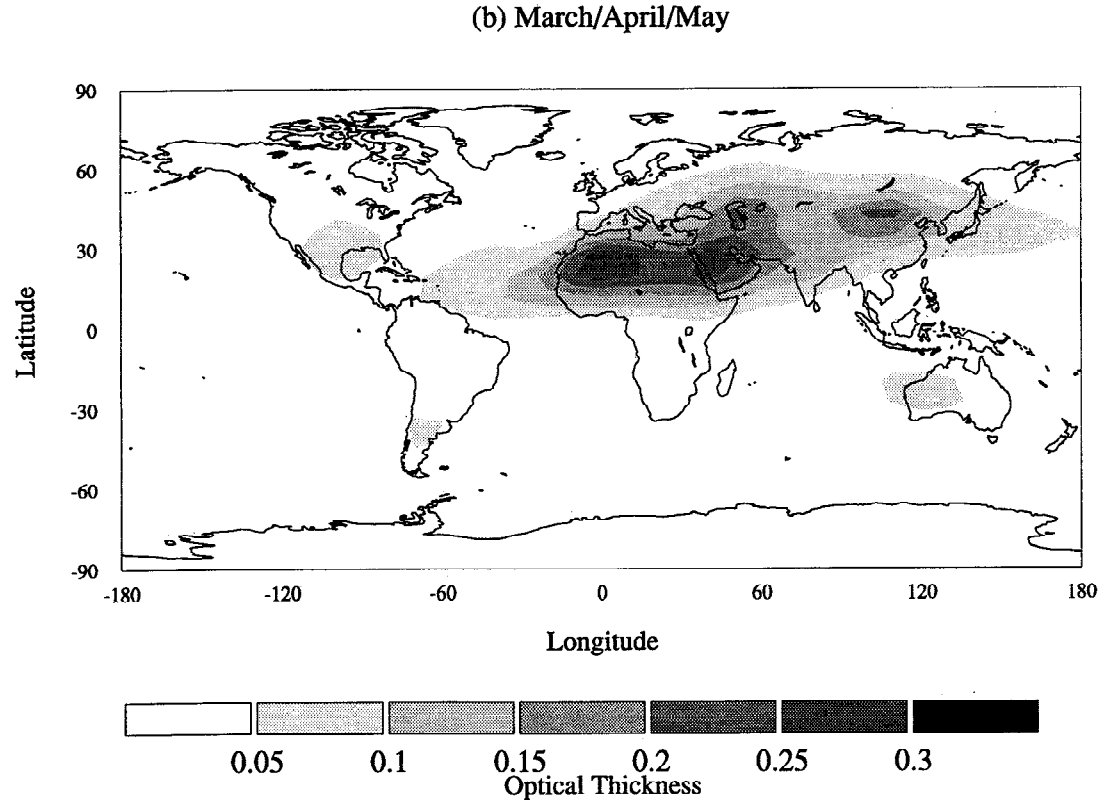

Figure 8. Modeled optical thickness for the four seasons. (a) December–February, (b) March–May, (c) June–August, and (d) September–November.

(c) June/July/August

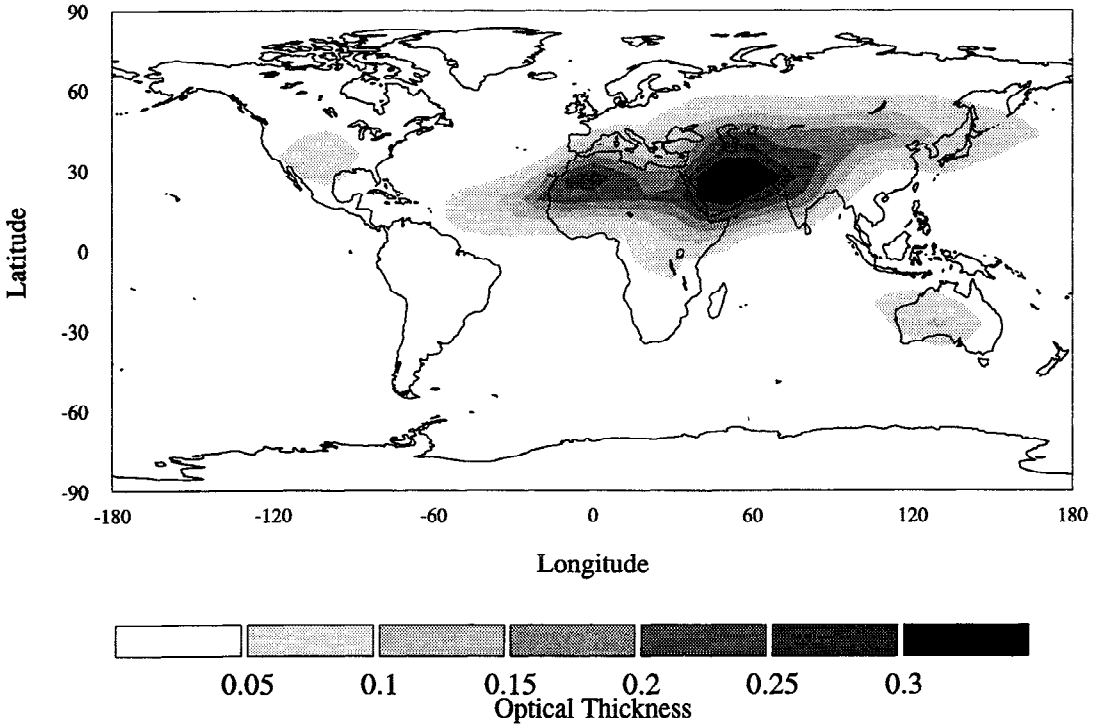

(d) September/October/November

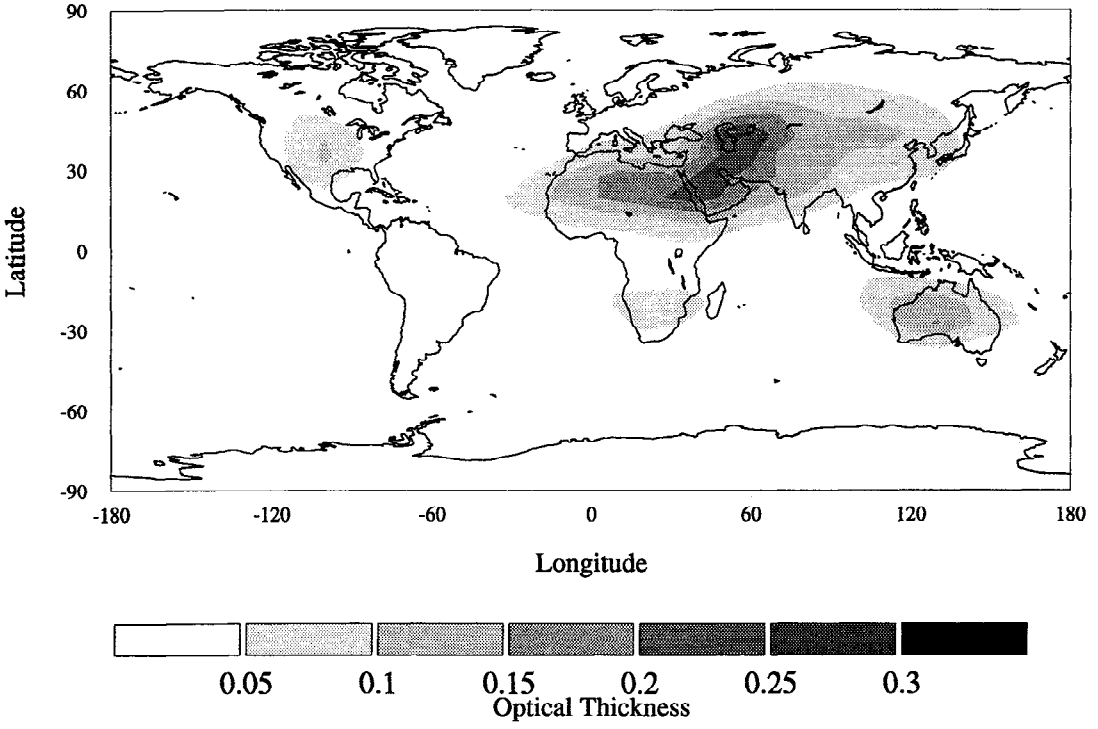

Figure 8. (continued)

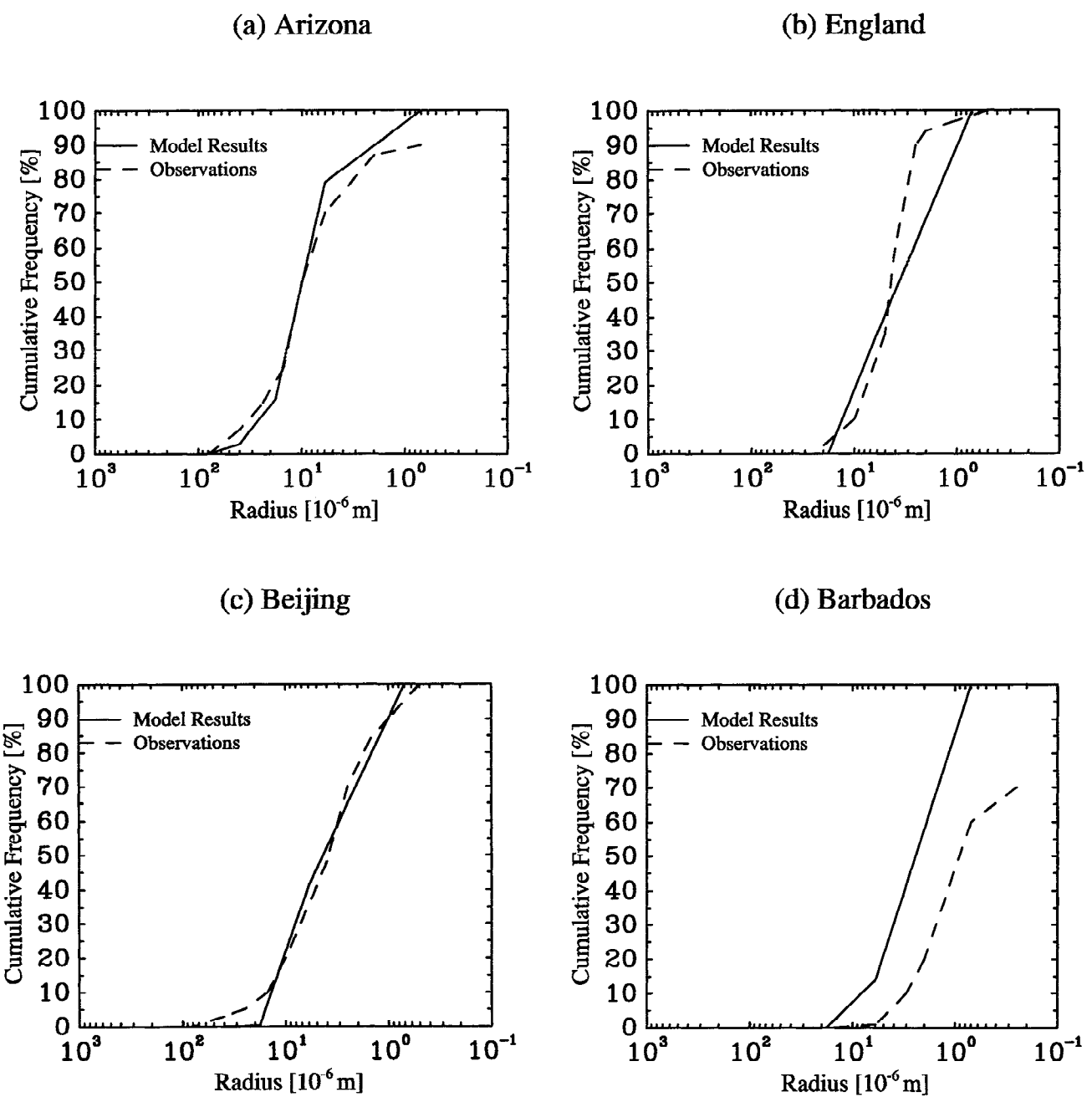

Figure 9. Comparision of cumulative dust size frequencies as calculated by the transport model with data reported by *Pye* [1987] at four sites.

4. Conclusion

In this paper we have presented a new model of mineral dust in the atmosphere which resolves the size distribution of mineral dust. Only dust sources from "undisturbed" deserts, grasslands, and shrub lands are included. Our best guess case yields a global dust source strength of 3000 Mt yr^{-1} which is composed of 390 Mt yr^{-1} clay, 1960 Mt yr^{-1} silt, and 650 Mt yr^{-1} sand. The dust model successfully describes the seasonality and deposition rates of mineral dust at the few locations where such observations have been made. The failure to reproduce the seasonal shift of the Saharan dust plume over the Atlantic Ocean highlights the importance of anthropogenic sources in the atmospheric mineral dust cycle. These sources include newly exposed soil surfaces due to desertification and disturbance of the soil by agricultural activities. The overestimate of the Australian dust source suggests that contrary to general assumptions, desert areas might not be the most important sources of dust, as in these regions the fine soil particles may have been blown out already. A more realistic mineral dust transport model must therefore include anthropogenic sources.

To obtain a better resolved range of optical thicknesses from the dust distributions, which is crucial

Table 3. Range of Possible Optical Thicknesses τ at Sites "Arizona" (A), "England" (B), "Beijing" (C), and "Barbados" (D) Due to Uncertainties in the Model Assumptions

Dust Source, Mt yr^{-1}	r_{eff} (Clay), μm	α_{clay}	τ (A)	τ (B)	τ (C)	τ (D)
1500–5000	0.6	1/6	0.03–0.08	0.01–0.04	0.05–0.2	0.02–0.06
3000	0.3–0.7	1/6	0.02–0.06	0.01–0.03	0.04–0.1	0.02–0.04
3000	0.6	1/6–1/50	0.01–0.05	0.003–0.02	0.02–0.1	0.01–0.04

α_{clay}, ratio of the mass available for uplift and the total mass of the clay fraction.

for radiative transfer calculations, more information is needed about the size spectra in the soils and about the processes of dust uplift in the size range $< 1\ \mu$m radius. We do not know which fraction of clay is agglomerated or whether there is a size limit below which no individual particles are removed from the soil. It is also unknown whether, in the case that clay is carried out of the ground as agglomerated particles or sticking to silt or sand particles [e.g., *Gillette et al.*, 1974; *Scheffer and Schachtschabel*, 1992], there are processes to separate the particles during the transport. Therefore it is not clear whether the differences in the particle size distributions observed at the dust source regions and far from those regions are caused by the different settling velocities alone or whether they are additionally affected by some unknown processes. This would not affect the total dust mass in the atmosphere, but would affect the optical thickness resulting from these dust concentrations. Without information about these processes the radiative properties of mineral dust cannot be ascertained with a degree of accuracy necessary for understanding climate change.

Acknowledgments. We thank R. Duce, J. Prospero, and H. Rodhe for very helpful comments on the manuscript and A. Lacis for advice about the optical thickness calculations. The work was supported by the NASA Office of the Mission to Planet Earth.

References

Adler, R. F., A. J. Negri, P. K. Keehn, and I. M. Hakkarinen, Estimation of monthly rainfall over Japan and surrounding waters from a combination of low-orbit microwave and geosynchronous IR data, *J. Appl. Meteorol.*, *32*, 335–356, 1993.

Berry, F. A., E. Bollay, and N. R. Beers, *Handbook of Meteorology*. McGraw-Hill, New York, 1945.

Betzer, P. R., et al., Long-range transport of giant mineral aerosol particles, *Nature*, *336*, 568–571, 1988.

Bouwman, A. F., I. Fung, E. Matthews, and J. John, Global analysis of the potential for N_2O production in natural soils, *Global Biogeochem. Cycles.*, *7*, 557–579, 1993.

Buat-Menard, P., and R. A. Duce, Precipitation scavenging of aerosol particles over remote marine regions, *Nature*, *321*, 508–510, 1986.

Charlson, R. J., J. Langner, H. Rodhe, C. B. Leovy, and S. G. Warren, Perturbation of the northern hemisphere radiative balance by backscattering from anthropogenic sulfate aerosols, *Tellus*, *43*AB, 152–163, 1991.

d'Almeida, G., and L. Schütz, Number, mass, and volume distribution of mineral aerosol and soils of the Sahara, *J. Clim. Appl. Meteorol.*, *22*, 233–243, 1983.

Duce, R. A., et al., The atmospheric input of trace species into the world ocean, *Global Biogeochem. Cycles*, *5*, 193–259, 1991.

Dulac, F., D. Tanre, G. Bergametti, P. Buat-Menard, M. Desbois, and D. Sutton, Assessment of African airborne dust mass over the western Mediterranean Sea using Meteosat data, *J. Geophys. Res.*, *97*, 2489–2506, 1992.

Fouquart, Y., B. Bonnel, M. Chaoui Roquai, R. Santer, and A. Cerf, Observations of Saharan aerosols: Results of the ECLATS field experiment, 1, optical thickness and aerosol size distribution, *J. Clim. Appl. Meteorol.*, *26*, 28–37, 1987.

Fung, I., K. Prentice, E. Matthews, and G. Russell, Three-dimensional tracer model study of atmospheric CO_2: Response to seasonal exchanges with the terrestrial biosphere, *J. Geophys. Res.*, *88*, 1281–1294, 1983.

Gao, Y., R. Arimoto, J. T. Merril, and R. A. Duce, Relationships between the dust concentrations over eastern Asia and the remote North Pacific, *J. Geophys. Res.*, *97*, 9867–9872, 1992.

Genthon, C., Simulations of desert dust and sea salt aerosols in Antarctica with a general circulation model of the atmosphere, *Tellus*, *44*, 371–389, 1992.

Gillette, D., A wind tunnel simulation of the erosion of soil: Effect of soil texture, sandblasting, wind speed, and soil consolidation on dust production, *Atmos. Environ.*, *12*, 1735–1743, 1978.

Gillette, D. A., I. H. Blifford, and D. W. Fryrear, The influence of wind velocity on the size distributions of aerosols generated by the wind erosion of soils, *J. Geophys. Res.*, *79*, 4068–4075, 1974.

Giorgi, F., A particle dry-deposition parameterization scheme for use in tracer transport models, *J. Geophys. Res.*, *91*, 9794–9806, 1986.

Goudie, A. S., Dust storms in space and time, *Prog. Phys. Geog.*, *7*, 502–530, 1983.

Hansen, J. E., G. L. Russell, D. Rind, P. Stone, A. Lacis,

S. Lebedeff, R. Ruedy, and L. Travis, Efficient three-dimensional global models for climate studies: Models I and II, *Mon. Weather Rev., 111*, 609–662, 1983.

Jaenicke, R., Über die Dynamik atmosphärischer Aitkenteilchen, *Ber. Bunsenges. Phys. Chem., 82*, 1198–1202, 1978.

Jankowiak, J. E., and P. A. Arkin, Rainfall variations in the Tropics during 1986–1989, as estimated from observations of cloud top temperature, *J. Geophys. Res., 96*, 3359–3373, 1991.

Jankowiak, I., and D. Tanre, Satellite climatology of Saharan dust outbreaks: Methods and preliminary results, *J. Clim., 5*, 646–656, 1992.

Joussaume, S., Three-dimensional simulations of the atmospheric cycle of desert dust particles using a general circulation model, *J. Geophys. Res., 95*, 1909–1941, 1990.

Junge, C. E., E. Robinson, and F. L. Ludwig, A study of aerosols in Pacific air masses, *J. Appl. Meteorol., 8*, 340–347, 1969.

Kalma, J. D., J. G. Speight, and R. J. Wasson, Potential wind erosion in Australia: A continental perspective, *J. Climatol., 8*, 411–428, 1988.

Kiehl, J. T., and B. P. Briegleb, The relative importance of sulfate aerosols and greenhouse gases in climate forcing, *Science, 260*, 311–314, 1993.

Littmann, T., Dust storm frequency in Asia: Climatic control and variability, *Int. J. Climatol., 11*, 393–412, 1991.

Mason, B. J., *The Physics of Clouds*. Oxford University Press, London, 1957.

Matthews, E., Atlas of archived vegetation, land use and albedo data sets, *NASA Tech. Rep., NASA TM-86199*, 53 pp., 1983.

McDonald, W. F., *Atlas of Climatic Charts of the Oceans*, USDA Weather Bureau, Washington, D. C., 1938.

Prather, M. J., B. McElroy, S. C. Wofsy, G. R. Russell, and D. Rind, Chemistry of the global troposphere: Fluorocarbons as tracers of air motion, *J. Geophys. Res., 92*, 6579–6613, 1987.

Prospero, J. M., and E. Bonatti, Continental dust in the atmosphere of the eastern equatorial Pacific, *J. Geophys. Res., 74*, 3362–3371, 1969.

Prospero, J. M., and R. T. Nees, Dust concentration in the atmosphere of the equatorial North Atlantic: Possible relationship to the Sahelian drought, *Science, 196*, 1196–1198, 1976.

Prospero, J. M., R. A. Glaccum, and R. T. Nees, Atmospheric transport of soil dust from Africa to South America, *Nature, 289*, 570–572, 1981.

Pye, K., *Aeolian Dust and Dust Deposits*. Academic, San Diego, Calif., 1987.

Rao, C. R. N., L. L. Stowe, E. P. McClain, J. Sapper, and M. P. McCormick, Development and application of aerosol remote sensing with AVHRR data from the NOAA satellites, in *Aerosols and Climate*, edited by P. V. Hobbs, A. Deepak, Hampton, Va., 1988.

Rossow, W. B., L. C. Garder, P. L. Lu, and A. Walker, International satellite cloud climatology project (ISCCP) documentation of cloud data, *WMO Tech. Rep., WMO/TD-266*, World Meteorol. Organ., Geneva, 78 pp., 3 appendices, 1991.

Russell, G. L., and J. A. Lerner, A new finite-differencing scheme for the tracer transport equation, *J. Appl. Meteorol., 20*, 1483–1498, 1981.

Scheffer, F., and P. Schachtschabel, *Lehrbuch der Bodenkunde*, 13th edition, F. Enke, Frankfurt, Germany, 1992.

Shao, Y., M. R. Raupach, and P. A. Findlater, Effect of saltation bombardment on the entrainment of dust by wind, *J. Geophys. Res., 98*, 12,719–12,726, 1993.

Shea, D., Climatological atlas: 1950–1979, surface air temperature, precipitation, sea level pressure, and sea surface temperature, *NCAR Tech. Rep., NCAR/TN-269+STR*, Natl. Cent. for Atmos. Res., Boulder, Co., 1986.

Sirokko, F., and M. Sarntheim, Wind-borne deposits in the northwestern Indian Ocean: Record of Holocene sediments versus modern satellite data, in *Paleoclimatology and Paleometeorology: Modern and Past Patterns of Global Atmospheric Transport*, edited by M. Leinen and M. Sarntheim, pp. 401–433, Kluwer Academic, 1989.

Swap, R. M., M. Garstang, S. Greco, R. Talbot, and P. Kallberg, Saharan dust in the Amazon basin, *Tellus, 44B*, 133–149, 1992.

Trenberth, K. E., and J. G. Olson, An evaluation and intercomparison of global analyses from NMC and ECMWF, *Bull. Am. Meteorol. Soc., 69*, 1047–1057, 1988.

U.S. Department of Agriculture, *Soil Taxonomy, Agr. Handb. 436*, Soil Conservation Service, U.S. Department of Agriculture, 1975.

Webb, R., C. Rosenzweig, and E. R. Levine, A global data set of particle size properties, NASA Tech. Rep., *NASA TM-4286*, 33 pp., 1991.

Zobler, L., A world file for global climate modeling, NASA Tech. Rep., *NASA TM-87802*, 32 pp., 1986.

I. Fung, School of Earth and Ocean Sciences, University of Victoria, P.O. Box 1700, Victoria, British Columbia, V8W 2Y2, Canada.

I. Tegen, Department of Applied Physics, Columbia University, 2880 Broadway, New York, N.Y. 10025.

(Received January 11, 1994; revised July 8, 1994; accepted July 22, 1994.)